Chalcogenide Letters Vol. 16, No. 8, August 2019, p. 395 - 403

ENHANCEMENT OF POWER FACTOR BY Sn DOPING IN $Tl_8Sb_{2-x}Sn_xTe_6$ NANO-CHALCOGENIDE SYSTEM

W. M. KHAN*, W. H. SHAH, M. TUFAIL, S. KHAN, W. A. SYED, N. AHMAD
Department of Physics, Faculty of Basic and Applied Sciences
International Islamic University, Islamabad, Pakistan

We have prepared the quaternary thermoelectric nanoparticles, thallium tin antimony telluride $Tl_8Sb_{2-x}Sn_xTe_6$ where the concentration of the Sn is (1.96, 1.97, 1.98, 1.99, 2.00) using the solid state reactions techniques. The nanoparticles have been prepared by the ball mining method. The Sn is doping in the quaternary compound which have changes their electrical and thermal properties. The crystal structure has been analyzed by the x-rays diffractometery (XRD), to determine the phase structure. The XRD data shows no extra peak; confirm the purity of the sample. The energy dispersive spectroscopy (EDX) shows the stoichiometric elemental ratio of the compound studied here. With the increasing concentration of the Sn in the compound, the electrical conductivity is decreases as temperature is increases while the Seebeck coefficient is increased as temperature is increases. At last, both electrical conductivity and Seebeck coefficient is increased. So that the power factor is also increased in the range of 300-550 K. The compound which has Sn concentration is 0.61, has the highest power factor at 550 K which is the 8.9 $\mu Wcm^{-1}K^{-2}$.

(Received April 24, 2019; Accepted August 11, 2019)

Keywords: Quaternary thermoelectric, Nanoparticles, Seebeck coefficient, Electrical Conductivity

1. Introduction

The chalcogenide compounds which are doped the metallic like properties become the semiconductors have the different applications in the thermoelectric appliances [1-7] solar volte's [8-11] different radiations detectors [12-14] and super capacitors [15-17]. Basically, there is insulators nature so there are different types of the chalcogenide materials found it [18-22]. Due to heavy atomic weight it has the marvelous properties like the low electrical conductivity for determining the detectors [19] and the low thermal and high electrical conductivity properties for the thermoelectric materials [20]. Our major aim is to change the chemistry of the chalcogenide material for benefits of the human beings. The thermoelectric materials is used to convert thermal energy into electrical energy [21, 23, and 24], in a reliable way [25]. The most common example is exhausted of gases from the cars. So that there are some thermoelectric materials are found like skutterides [26] lead telluride [27] half Haussler's compound [28].

The motivation of thallium based compounds are; i) due to the heavy atomic weight so that it is reducing the thermal conductivity and ii) creating the complex behavior due to their lone pair of it which helps to create the different properties of compounds e.g., TI_9SbTe_6 [29] Tl_9BiTe_6 [30] $Tl_{10-x}Sn_XTe_6$ [31] $TlBiTe_2$ [32] $TlSbTe_2$ [33] and Tl_9AgTe_5 [34].

The prime reason of this project is to design and fabricate such nano-materials system which are more efficient, i.e. have high power factor and environment friendly. The effectiveness of the material can be evaluated by the figure of merit $ZT=TS^2\sigma\kappa^{-1}$ where S is the Seebeck coefficient, σ is the electrical conductivity, κ is the thermal conductivity and T is the difference of the temperature [36]. If the figure-of-merit is high, it has high efficiency that of converting the thermal energy into electrical energy. The figure of merit is depend on the high Seebeck and electrical conductivity while low thermal conductivity. So the narrow band gap doped semiconducting nano-system will be the best option [35].

*Corresponding author: waqaskhanrwp@yahoo.com

2. Experiment

The Sn doped $Tl_8Sb_{2-x}Sn_xTe_6$ is (x=1.96, 1.97, 1.98, 1.99, 2.00) has been prepared by solid state reactions in evacuated sealed silica tubes. The purpose of this study was mainly for discovering new type of ternary and quaternary compounds by using Tl^{+1}, Sn^{+3} and Te^{-2} elements as the starting materials. Direct synthesis of stoichiometric amount of high purity elements i.e. 99.99% of different compositions have been prepared for preliminary investigations. Since most of these starting materials for solid reactions are sensitive to oxygen and moistures, they were weighing stoichiometric reactant and transferring to the silica tubes in the gloves box which is filled with Argon. Then, all constituents were sealed quartz. Before putting these samples in the resistance furnace for the heating, the silica tube putting in vacuum line to evacuate the argon and then sealed it. This sealed powder were heated up 650 ^{0}C at a rate not exceeding 1 k/mint and kept at the temperature for 24 hours. The sample was cooled down with extremely slow rate to avoid quenching, dislocations, and crystals deformation. Structural analysis of all these samples was carried out by X-rays diffraction, using an Intel powder diffract meter with position- sensitive detector and CuKα radiations at room temperature. No additional peaks were detected in any of the sample presenting here, confirms the single phase composition of these prepared nano-particles. The SEM shows the nanoparticle was prepared and EDX data shows that the statistically ratio of element in compound. The temperature dependence of Seebeck coefficient was measured for all these compounds on a cold presses pellet in rectangular shape, of approximately 5x1x1 mm^3 dimensions. The sensitivity of these samples was checked (for one sample) by measuring the thermoelectric power and confirmed that these samples are not sensitive to air. This sample exposes to air more than a week, but no appreciable changes observed in the Seebeck values. The pellet for these measurements was annealed at 400C^0 for 6 hours. For the electrical transport measurements 4-probe resistivity technique was used and the pellets were cut into rectangular shape with approximate dimension of 5x1x1mm^3.

3. Result and discussion

Fig. 1 shows the XRD pattern for the samples at the temperature 650 ^{0}C of the thallium antimony tin telluride's nano-particles, $Tl_8Sb_{2-x}Sn_xTe_6$ which were doping concentration is (x = 1.96, 1.97, 1.98, 1.99, 2) and calculated the crystal structure of the $Tl_8Sb_{2-x}Sn_xTe$. The highest intensity peak is at 31.80^0 with (213) plane orientation. It specifies that our nanoparticle is tetragonal phase which are laying all the doping concentrations. The crystallographic planes are observed at (130), (121), (220), 024), (006), (240), (413), (044) and (136) orientations. The XRD diffractometery result shows that the nano-particle $Tl_8Sb_{2-x}Sn_xTe_6$ is a single phase. Furthermore, the crystallites size can be determined by the Debye-Scherer formula, ($D = 0.9\lambda/\beta\cos\theta$) [37]. We have observed that the crystallite size of $Tl_8Sb_{2-x}Sn_xTe_6$ nanoparticles calculated is in the range of (21-25 nm), indicating that Sn incorporations in nanoparticles of $Tl_8Sb_{2-x}Sn_xTe_6$ do not affect significantly to its crystallite size.

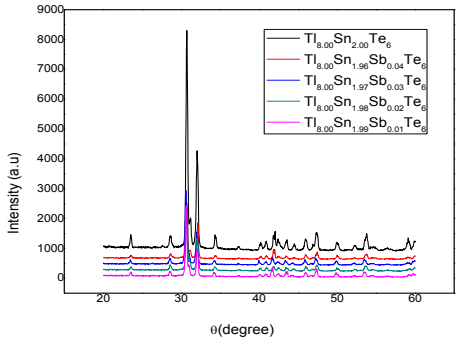

Fig. 1. XRD data $Tl_8Sb_{2-x}Sn_xTe_6$ with Sn (x =1.96, 1.97, 1.98, 1.99 and 2.00) collected at room temperature.

Table 1. Value of crystallite size and crystal system.

Sample	Crystallite size, $D = 0.9\lambda/\beta\cos\theta$ (nm)	Lattice constant a, b ,c = (Å)	Volume (Å^3)
$Tl_{8.00}Sb_{0.04}Sn_{1.96}Te_6$	25.248	a = b = 8.8931 c = 13.0050	1004.52
$Tl_{8.00}Sb_{0.03}Sn_{1.97}Te_6$	21.794	a = b = 8.8452 c = 13.0756	1023.97
$Tl_{8.00}Sb_{0.02}Sn_{1.98}Te_6$	21.171	a = b = 8.8245 c = 13.000	1013.47
$Tl_{8.00}Sb_{0.01}Sn_{1.99}Te_6$	21.119	a = b = 8.8101 c = 13.0012	1009.07
$Tl_{8.00}SbSn_2Te_6$	21.456	a = b = 8.8485 c = 13.1627	1022.73

The X-ray diffraction techniques doesn't find the exact ratio of elements present in nanoparticles of $Tl_8Sb_{2-x}Sn_xTe_6$. In Fig. 2, spectra show the morphology of nanoparticles of $Tl_8Sb_{2-x}Sn_xTe_6$ which are in the range of 100 nm. The Energy Dispersive X-Rays spectroscopy (EDX) is used for the elemental as well as for the compositional analysis. The EDX spectroscopy shows the ratio or quantitative percentage of the elements present in the nano-particles. For nanoparticles $Tl_8Sb_{0.04}Sn_{1.96}Te_6$ has a single phase which is highly rich in thallium (69.9 % Tl, 25.8 % Te, 3 % Sn and 1.2% Sb) for every element in the nano-particles. The atomic percent (% At) of nanoparticles at numerous points have the different crystal for a special sample. It has averaged and related to the nominated atomic percent of the corresponding nano-particles. In Fig. 3, the spectra show the Tl:Te ratio and the Sn concentration appear in the nano-particles.

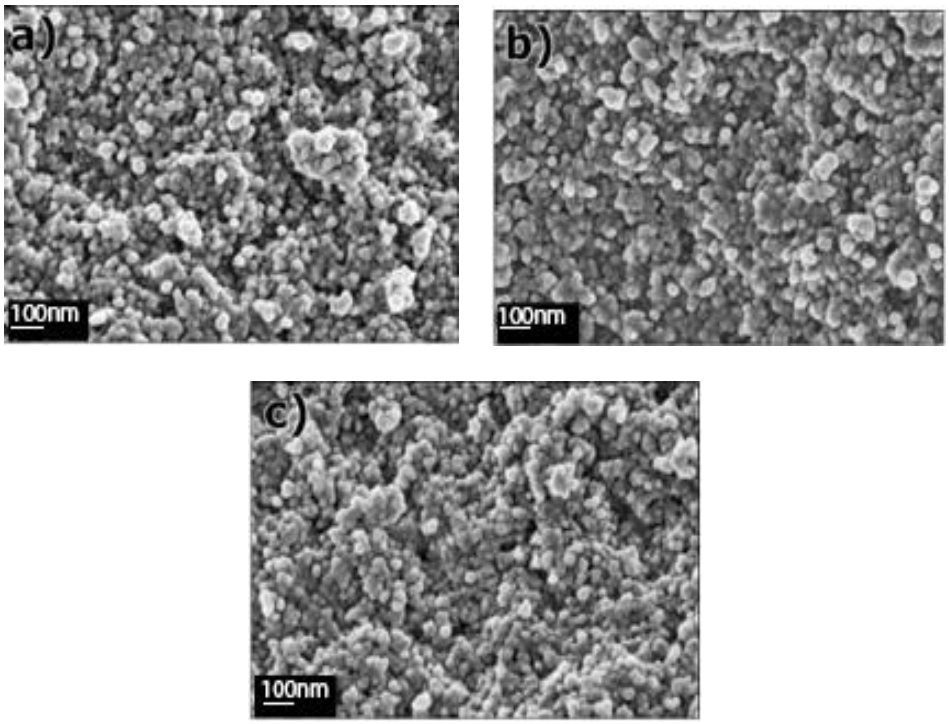

Fig. 2. $Tl_8Sb_{2-x}Sn_xTe_6$ SEM images of (x =1.96, 1.97, 1.98 and 1.99).

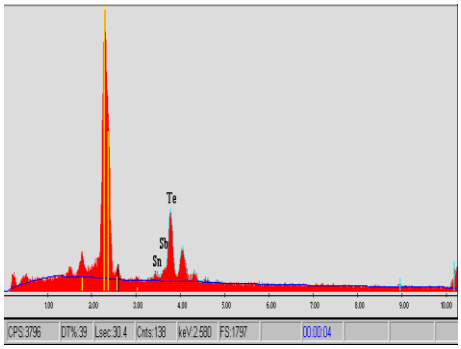

Fig. 3. $Tl_8Sb_{2-x}Sn_xTe_6$ EDX images (x =1.96, 1.97, 1.98 and 1.99).

Table 2. EDX Statistical ratio of elements in compound.

Element	Wt %	At %
Sn	2.58	3.73
Sb	2.82	3.97
Te	25.60	34.41
Tl	69.00	57.89

The thermal dependence of electrical conductivity for the Nano-particles $Tl_8Sb_{2-x}Sn_xTe_6$ for composition (where x=1.96-1.99) has been studied in the range of 300-550 K. We have observed that electrical conductivity **σ** decreases as temperature increases, behave like metal doped semiconducting system as expected. The behavior of Sn doped in $Tl_8Sb_{2-x}Sn_xTe_6$ system is true in case of intrinsic semi-conductors with concentration of x=*1.96* as well as for doped semiconductors with *x* up to 1.99. The trend of decreasing the electrical conductivity as increasing the temperature indicates that our nanoparticles $Tl_8Sb_{2-x}Sn_xTe_6$ has the p-type conductivity.

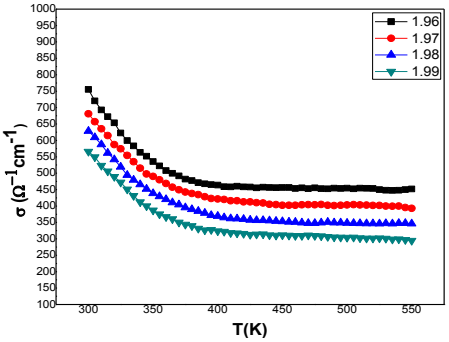

Fig. 4. Temperature dependence of electrical conductivity of $Tl_8Sb_{2-x}Sn_xTe_6$ (x =1.96, 1.97, 1.98 and 1.99) of the cooled pressed pellet with heating profile.

Fig. 4 shows that the nanoparticles of $Tl_8Sb_{0.04}Sn_{1.96}Te_6$ has the highest value of electrical conductivity i.e. 755.05 $\Omega^{-1}cm^{-1}$ at 300 K, which is decreases as increasing the temperature, till to 454.61 $\Omega^{-1}cm^{-1}$ at 550 K. The electrical conductivity of $Tl_8Sb_{2-x}Sn_xTe_6$ also decreases with increasing doping concentration of *x*. For example, the concentration of the nanoparticle is change from x=1.96 to 1.99, the electrical conductivity of the nanoparticle was decreased from 755.05 Ω^{-}

$^{1}cm^{-1}$ to 566.06 $\Omega^{-1}cm^{-1}$ at 300 K. Similarly, at 550 K, it decreased from 454.61 $\Omega^{-1}cm^{-1}$ to 303.75 $\Omega^{-1}cm^{-1}$.

Table 3. Temperature dependence of the Electrical Conductivity of all $Tl_8Sb_{2-x}Sn_xTe_6$ samples at 300 and 550 K.

Sample	Electrical conductivity $\Omega^{-1}cm^{-1}$ at 300 K	Electrical Conductivity $\Omega^{-1}cm^{-1}$ at 550 K
$Tl_8Sb_{0.04}Sn_{1.96}Te_6$	755.05	454.61
$Tl_8Sb_{0.03}Sn_{1.97}Te_6$	681.22	403.30
$Tl_8Sb_{0.02}Sn_{1.98}Te_6$	628.51	348.32
$Tl_8Sb_{0.01}Sn_{1.99}Te_6$	566.06	303.75

The thermal dependency of the Seebeck coefficient (S) measured for $Tl_8Sb_{2-x}Sn_xTe_6$ nano-systems with different concentration of Sn (x=1.96, 1.97, 1.98, 1.99, 2.00) has been shown in figure 4. We have observed that the Seebeck coefficient is increasing as the temperature is increase for the samples studied here. The values of Seebeck co-efficient for $Tl_8Sb_{0.04}Sn_{1.96}Te_6$ is increased from S = 297.18 μVK^{-1} at 300 K to S = 566.06 μVK^{-1} at 550 K, similarly for $Tl_8Sb_{0.03}Sn_{1.97}Te_6$ the values of S varies as 347.58 μVK^{-1} at 300 K to 628.51 μVK^{-1} at 550 K. For $Tl_8Sb_{0.02}Sn_{1.98}Te_6$ the Seebeck coefficient is increased from S = 395.64 μVK^{-1} at 300 K to 681.22 μVK^{-1} at 550 K, and for $Tl_8Sb_{0.01}Sn_{1.99}Te_6$, 433.28 μVK^{-1} at 300 K to 725.76 μVK^{-1} at 550 K. It shows that the Seebeck Coefficient gradually increased as Sn concentration increases in $Tl_8Sb_{2-x}Sn_xTe_6$ nano-system. At 300 K, it is enhanced from 297.18 μVK^{-1} at *x = 1.96* to *433.28 μVK^{-1} at x =1.99*. Similarly, by increasing Sn from x = 1.96 to 1.99, S increased from 566.06 μVK^{-1} to 725.76 μVK^{-1} at 550 K. The Seebeck coefficient is depend on the temperature. Due to the doping of the P type materials in the nanomaterials, it is increases the Seebeck coefficient. This implies that the major carrier are in the nanomaterials are the holes.

Experimentally we have observed that the Seebeck co-efficient increases with temperature for $Tl_8Sb_{2-x}Sn_xTe_6$ nano-samples studied here. In previous study, heavy metals which have P-type deficiency, is observed in such as telluride's system, as also found in $Tl_{10-x}Ln_xTe_6$ series and Tl_9BiTe_6, which is causing a highly number of charge carriers (> 10^{19} cm^{-3}). Due to this, $Tl_{10-x}Ln_xTe_6$ series (Ln = La, Ce, Pr, Nd, Sb, Sm, Gd, Tb) having almost similar trend of Seebeck coefficient of $Tl_{10-x}Sb_xTe_6$ [7], as increasing the Seebeck coefficient with temperature it creates the smaller energy band gaps (E_g), which can be easily excited from the valance band to conduction band.

The temperature dependency with the variation in concentration, can be attributed to the relationship between Seebeck coefficient and temperature and charge carrier concentration according to the following mathematical expression [17],

$$S = T\frac{8\pi^2 k_B^2 m^*}{3eh^2}\left(\frac{\pi}{3n}\right)^{\frac{2}{3}}. \quad (1)$$

Where, T is temperature, k_B is Boltzmann constant, e is electronic charge, h is Planck constant, m^* is effective mass, and n is charge carrier concentration in system.

The equation (1) shows that, S is directly proportional to T, but at the same time, it is inversely proportional to n; therefore, overall S would depend on which parameter dominates in a particular situation for a specific system. Compounds with $x \geq 1$ is supposed to be p-type semiconductor as $Tl_8Sb_{2-x}Sn_xTe_6$ is an intrinsic semiconductor observed from the experimental positive value of S in the system studied here. As electrical conductivity, σ, increases with increases in n according to the equation $\sigma = n e \mu$, where μ = carrier mobility and e = charge of carriers and as mentioned above, S has $n^{-2/3}$ dependence, S and σ are related inversely through n. Therefore, the opposite observation is expected for the σ trend. The experimental results endorse

this expectation as x increases, σ decreases for a given Sn due to decrease in n (see Fig. 3). Furthermore, as T increases, σ decreases, because $\mu = \tau / m^*$ where τ is the relaxation time, which decreases with increasing temperature.

Table 4. Temperature dependence of the Seebeck coefficient of all $Tl_8Sb_{2-x}Sn_xTe_6$ samples at 300 and 550 K.

Sample	Seebeck coefficient(μVK^{-1}) at 300 K	Seebeck coefficient(μVK^{-1}) at 550 K
$Tl_8Sb_{0.04}Sn_{1.96}Te_6$	297.18	566.06
$Tl_8Sb_{0.03}Sn_{1.97}Te_6$	347.58	628.51
$Tl_8Sb_{0.02}Sn_{1.98}Te_6$	395.64	681.22
$Tl_8Sb_{0.01}Sn_{1.99}Te_6$	433.28	725.76

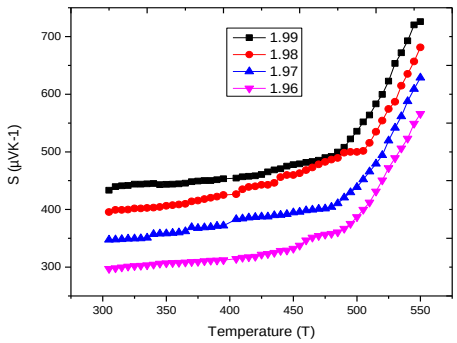

Fig. 5(a). Temperature dependence of Seebeck coefficient of $Tl_8Sb_{2-x}Sn_xTe_6$ (x =1.96, 1.97, 1.98 and 1.99) of the cooled pressed pellet with heating profile.

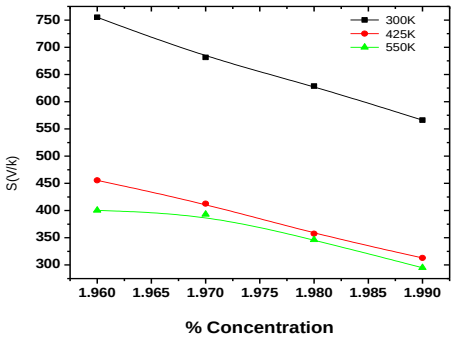

Fig. 5(b). %Concentration dependence of Seebeck Coefficient of $Tl_8Sb_{2-x}Sn_xTe_6$ (x =1.96, 1.97, 1.98 and 1.99) of the cooled pressed pellet with heating profile.

As it is significant non-linear electrical and thermal dependency is observed from 300 to 550 K, showing the decomposition of the semiconducting network into non-metallic clusters which are supported by a study of the transport and thermal characteristics. This investigation further testifies that the semi-conducting state becomes suppressed with the doping of Sn, which is the clear evidence of increase of Seebeck co-efficient.

Power Factor

The power factor, characterized by S^2 σ, shows overall thermoelectric performance of thallium tin antimony telluride $Tl_8Sb_{2-x}Sn_xTe_6$ nanoparticles. The power factor increases with increasing temperature for all of the samples studied here which are mainly attributed to increasing Seebeck coefficients. The Sn doped system shows a power factor values in the range of 2.21 to 8.9 μW-cm^{-1}K^{-2} at 300 K and 550 K respectively. The samples with (x =1.96, 1.97, 1.98 and 1.99) show slight increasing with less dependence on temperature and aggregate at same point at 4.0 μW-cm^{-1}K^{-2} as shown in Fig. 5. All the samples have shown better performance of power factor as compared to un-doped system. Tl_9LnTe_6 series as reported that the doping of different elements i.e. (Ce, Pr) in ternary group show different values of power factor occur in the range of 2.8-4.6 μWcm^{-1}K^{-2}at 550 K. Ternary group ($Tl_{10}SnTe_6$) substitute of Sn has reported the value of power factor at x = 1.96 are 3.6-4.9 μWcm^{-1}K^{-2} at 320 K and 550 K respectively [18-19] which is quite low value compared to the one reported in the present study, i.e. for Nano-particles $Tl_8Sb_{0.04}Sn_{1.96}Te_6$ system power factor is 8.9 μWcm^{-1}K^{-2} at 550 K. This was the objective of this research work to enhance the power factor and thermoelectric properties in modified nano-system of $Tl_{10}Te_6$ as compared to their bulk counter-part.

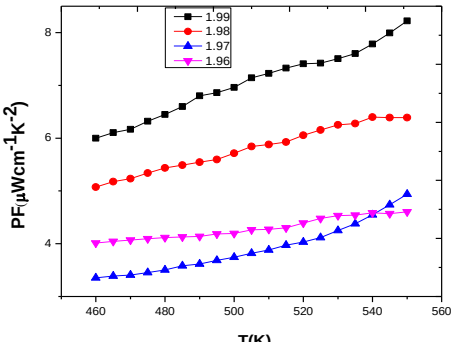

Fig. 6(a). Temperature dependence of Power Factor of $Tl_8Sb_{2-x}Sn_xTe_6$ (x =1.96, 1.97, 1.98 and 1.99) of the cooled pressed pellet with heating profile.

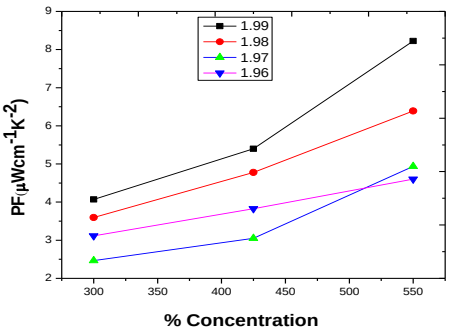

Fig. 6(b). %Concentration dependence of Power Factor of $Tl_8Sb_{2-x}Sn_xTe_6$ (x =1.96, 1.97, 1.98 and 1.99) of the cooled pressed pellet with heating profile.

4. Conclusions

Various concentrations of Sn doped $Tl_8Sb_{2-x}Sn_xTe_6$ compounds series were synthesized, and their physical properties were studied for x=1.96,1.97,1.98,1.99. These nano-materials are single phase as confirmed by x-rays diffractometry and the crystal structure of $Tl_8Sb_{2-x}Sn_xTe_6$ was determined with the experimental formula, possessing the same space group 14/mcm as Tl_5Te_3. The thermoelectric properties of polycrystalline $Tl_8Sb_{2-x}Sn_xTe_6$compounds were measured in the temperature range of 300-550 K. The Seebeck

coefficient is positive in the whole temperature range, and is increasing with increase in temperature, conferring that hole conduction dominates in these types of nano-system.

For higher concentrations of Sn, the Seebeck co-efficient of the doped tellurium telluride is decreasing due to increasing hole concentration which in turns increasing the electron scattering in this Sn doped chalcogenide nano-system. On the other hand when the amount of Sn doping is more than1.98, the Sn doping will increase the carrier's density. However, the smaller grains upon Sn concentrations will enhance the electron scattering, resulting increase in thermos-power. Further improvements appear to be possible by optimizing the materials on both the micro and nano-level.. Moreover, different partial substitutions may optimize, or decrease the performance, with different dopants, which remains to be investigated. This is an investigation for the optimization of Sn dopants concentration to achieve desirable thermoelectric properties and to optimize different physical properties in Sn doped $Tl_8Sb_{2-x}Sn_xTe_6$ chalcogenide nano-system.

References

[1]. G. J. Tan, L. D. Zhao, M. G. Kanatzidis, Chem. Rev. **116**, 12123 (2016).

[2] L.-D. Zhao, S.-H. Lo, Y. Zhang, H. Sun, G. Tan, C. Uher, C. Wolverton, V. P. Dravid, M. G. Kanatzidis, Nature **508**, 373 (2014).

[3] K. Biswas, J. He, I. D. Blum, C.-I. Wu, T. P. Hogan, D. N. Seidman, V. P. Dravid, M. G. Kanatzidis, Nature **489**, 414 (2012).

[4] J. P. Heremans, V. Jovovic, E. S. Toberer, A. Saramat, K. Kurosaki, A. Charoenphakdee, S. Yamanaka, G. J. Snyder, Science **321**, 554 (2008).

[5] J. P. Heremans, B. Wiendlocha, A. M. Chamoire, Energy Environ. Sci. **5**, 5510 (2012).

[6] Y. Pei, Z. M. Gibbs, A. Gloskovskii, B. Balke, W. G. Zeier, G. J. Snyder, Adv. Eng. Mater. **4**, 1400486 (2014).

[7] G. Tan, F. Shi, S. Hao, L.-D. Zhao, H. Chi, X. Zhang, C. Uher, C. Wolverton, V. P. Dravid, M. G. Kanatzidis, Nat. Commun. **7**, 12167 (2016).

[8] G. Tan, F. Shi, H. Sun, L.-D. Zhao, C. Uher, V. P. Dravid, M. G. Kanatzidis, J. Mater. Chem. A **2**, 20849 (2014).

[9] G. J. Snyder, E. S. Toberer, Nat. Mater. **7**, 105 (2008).

[10] S. Bag, O. Gunawan, T. Gokmen, Y. Zhu, D. B. Mitzi, Chem. Mater. **24**, 4588 (2012).

[11] H. Dittrich, A. Bieniok, U. Brendel, M. Grodzicki, D. Topa, Thin Solid Films **515**, 5745 (2007).

[12] P. Jackson, D. Hariskos, E. Lotter, S. Paetel, R. Wuerz, R. Menner, W. Wischmann, M. Powalla, Prog. in Photovoltaics **19**, 894 (2011).

[13] S. C. Riha, B. A. Parkinson, A. L. Prieto, J. Am. Chem. Soc. **131**, 12054 (2009).

[14] T. K. Todorov, K. B. Reuter, D. B. Mitzi, Adv. Mater. **22**, E156 (2010).

[15] J. Androulakis, S. C. Peter, H. Li, C. D. Malliakas, J. A. Peters, Z. Liu, B. W. Wessels, J.-H. Song, H. Jin, A. J. Freeman, M. G. Kanatzidis, Adv. Mater. **23**, 4163 (2011).

[16] S. Johnsen, Z. Liu, J. A. Peters, J.-H. Song, S. C. Peter, C. D. Malliakas, N. K. Cho, H. Jin, A. J. Freeman, B. W. Wessels, M. G. Kanatzidis, Chem. Mater. **23**, 3120 (2011).

[17] P. L. Wang, Z. F. Liu, P. Chen, J. A. Peters, G. J. Tan, J. Im, W. W. Lin, A. J. Freeman, B. W. Wessels, M. G. Kanatzidis, Adv. Funct. Mater. **25**, 4874 (2015).

[18] H. Chen, J. Jiang, L. Zhang, H. Wan, T. Qi, D. Xia, Nanoscale **5**, 8879 (2013).

[19] W. Du, Z. Zhu, Y. Wang, J. Liu, W. Yang, X. Qian, H. Pang, RSC Adv. **4**, 6998 (2014).

[20] S. Peng, L. Li, C. Li, H. Tan, R. Cai, H. Yu, S. Mhaisalkar, M. Srinivasan, S. Ramakrishna, Q. Yan, Chem. Comm. **49**, 10178 (2013).

[21] G. Wang, L. Zhang, J. Zhang, Chem. Soc. Rev. **41**, 797 (2012).

[22] H. B. Zhang, J. D. Yao, J. M. Shao, G. W. Yang, J. Phys. D., Appl. Phys. **49**, (2016).

[23] Y. L. Chen, Z. K. Liu, J. G. Analytis, J. H. Chu, H. J. Zhang, B. H. Yan, S. K. Mo, R. G. Moore, D. H. Lu, I. R. Fisher, S. C. Zhang, Z. Hussain, Z. X. Shen, Phys. Rev. Lett. **105**, 266401 (2010).

[24] H. Lin, R. S. Markiewicz, L. A. Wray, L. Fu, M. Z. Hasan, A. Bansil, Phys. Rev. Lett.

105, 036404 (2010).
[25] M. G. Kanatzidis, Chem. Mater. **22**, 648 (2009).
[26] G. Bourhis, P. Leduc, Oil Gas Sci. Technol. **65**, 39 (2010).
[27] M. Xie, D. M. Gruen, J. Phys. Chem. B **114**, 14339 (2010).
[28] J. Baxter, Z. Bian, G. Chen, D. Danielson, M. S. Dresselhaus, A. G. Fedorov, T. S. Fisher, C. W. Jones, E. Maginn, U. Kortshagen, Energy Environ. Sci. **2**, 559 (2009).
[29] D. Kraemer, B. Poudel, H. P. Feng, J. C. Caylor, B. Yu, X. Yan, Y. Ma, X. Wang, D. Wang, A. Muto, Nat. Mater. **10**, 532 (2011).
[30] G. Min, D. M. Rowe, Solid-State Electron. **43**, 923 (1999). 2006.29. C. Wood, Rep. Prog.
[31] G. S. Nolas, G. A. Slack, S. B. Schujman, Semicond. Semimet. **69**, 255 (2000).
[32] B. C. Sales, D. Mandrus, R. K. Williams, Science **272**, 1325 (1996).
[33] G. S. Nolas, M. Kaeser, R. T. Littleton, T. M. Tritt, Appl. Phys. Lett. **77**, 1855 (2000).
[34] D. T. Morelli, G. P. Meisner, J. Appl. Phys. **77**, 3777 (1995).
[35] C. Uher, Semicond. Semimet. **69**, 139 (2000).
[36] Y. Pei, X. Shi, A. D. LaLonde, H. Wang, L. D. Chen, G. J. Snyder, Nature **473**, 66 (2011).
[37] Glusker, Jenny Pickworth, Kenneth N. Trueblood, "Crystal Structure Analysis: A Primer." Oxford University Press, **14**, (2010).